The Avoided Crossing in the Normal-Mode Frequencies of a Wilberforce Pendulum

Thomas S. Wilhelm, Josh Orndorff, and D. A. Van Baak

Department of Physics and Astronomy,
Calvin College,
Grand Rapids, MI 49546 USA

Abstract:

The Wilberforce pendulum has long provided a favorite, and highly visual, method for displaying the energy interchange between coupled oscillations, but here we show that it is also suited to detailed quantitative measurement and modeling of coupled-oscillator phenomena. We make a careful numerical model of the user-variable rotational inertia of a commercial Wilberforce apparatus, and measure the two normal-mode oscillation frequencies of the system over a wide range of inertia settings. The observed mode frequencies match the theoretical predictions for coupled oscillators, and can be used to determine the model's (three) parameters with remarkable precision. The mode frequencies' variation with rotational inertia reveals a characteristic 'avoided crossing' seen generically in systems of coupled oscillators.

I. Introduction

The Wilberforce pendulum has served for generations as a delightful and very visible method for demonstrating some of the phenomena of coupled oscillators. In its typical form, it consists of a helical spring, fixed at its top end, and supporting a mass on its free lower end. Such a system can undergo simple harmonic motion in a translational mode (with the mass moving up and down), or in a torsional mode (with the mass rotating about a vertical axis). If the rotational inertia of the mass is properly chosen (so that these two frequencies would match), then the motion of the system is strikingly counter-intuitive, as it displays the repetitive and complete interchange of energy between the translational and rotational motions of the system.

Lionel Wilberforce invented this pendulum and published[1] his discovery in 1894. In that and subsequent treatments[2], the background was the theory of elasticity for the spring material, and the motivation was to use measureable properties of the pendulum's motion to infer elastic constants for the spring material. In particular, the energy interchange rate can be used to extract Poisson's ratio[3] for the spring material.

This paper has a somewhat different aim. Rather than go into the depths of elasticity theory, it seeks to cover some of the breadth of coupled-oscillator phenomena, using the Wilberforce pendulum as an example especially accessible to measurement and modeling. So here we make no attempt to derive, from the parameters of the spring as a whole, any elastic properties of its material. Rather, we seek to display results that

are generic to other systems of coupled oscillators, including ones lacking any connection to elasticity.

The dramatic interchanges of energy (from 100% translational to 100% rotational and back again) that can be demonstrated in a Wilberforce pendulum have always created an incentive to achieve the 'ideal tuning' that is necessary for this full interchange. But a fixation on this tuning condition can hide from view all the *other* coupled-oscillator phenomena that can be demonstrated with this device. Though ideal tuning is required for the full energy interchange, all the other phenomena of coupled oscillators occur at *any* value of the tuning. In particular, for any value of tuning, the system possesses, and can be arranged to display, its two normal modes. These normal modes, the 'eigenstates' of classical mechanics, have oscillation frequencies, and mode compositions, that can be readily measured, and theoretically modeled, over a wide range of tuning.

Two previous articles[4, 5] in this Journal have dealt with the very apparatus[6] we have also used for taking data. Together they deal more than adequately with connections to elasticity theory, and the description of the beat phenomenon at ideal tuning. Here we make systematic use of the user-variable rotational inertia of the pendulum bob in a commercial realization of Wilberforce's pendulum, and show that the system's rotational inertia can be varied over a factor-of-two range. Over that range, we've studied the frequencies, and the compositions, of the normal modes; and within that range, we have found, and modeled in precise

detail, the 'avoided crossing' which shows up in all sorts of systems of coupled oscillators.

We lay out an adequate amount of theory in section II, and describe our experimental procedures in section III. Guided by the theoretical development, we analyze in section IV the experimental data, to test in detail the theoretical predictions, and to extract the values of the system's parameters. In section V we use the Wilberforce-pendulum results to generalize to coupled-oscillator phenomena across classical mechanics, and even beyond. There we also discuss broadly applicable concepts, such as 'avoided crossing' and 'adiabatic transfe', which emerge very concretely and naturally from the work described here on the Wilberforce pendulum.

II. Theory

The Wilberforce pendulum that we've studied provides a near-perfect realization of the simplest system of coupled oscillations. We suppose that the state of the system can be described by a vertically-oscillating z-coordinate, and a torsionally oscillating θ-coordinate measuring rotation about the z-axis, and we ignore all its other degrees of freedom. We suppose that a mass m and a rotational inertia I can be defined by their appearance in a kinetic-energy expression

$$T = \frac{1}{2} m (\frac{dz}{dt})^2 + \frac{1}{2} I (\frac{d\theta}{dt})^2 \ , \qquad (1)$$

where a center-of-mass theorem assures us of the absence of any cross term. We also model the elastic potential energy of the system by the simplest possible quadratic form in the coordinates,

$$V = \frac{1}{2} k z^2 + \frac{1}{2} \kappa \theta^2 + \varepsilon z \theta \quad . \tag{2}$$

Here k gives the Hooke's-Law spring constant for vertical extension (without rotation), and κ gives the torsional constant of the spring (in the absence of extension). Finally, we use ε to describe the coupling constant between extension, and torsion, of the spring, which arises because of its helical winding. The units of k, κ, and ε are N/m, N.m, and N respectively. All three constants could be derived from a more fundamental treatment of the elasticity of the material of the spring, but we regard them as constants describing the spring empirically.

We note that the quadratic form V(z, θ) is a positive-definite quantity, provided that $\varepsilon^2 < k \kappa$ (as we will find it to be). Then the system's minimum energy, T + V, would come with both coordinates at rest at value zero. This, however, ignores the actual environment of Wilberforce demonstrations, conducted as they are in a uniform gravitational field. In actual fact, the system's potential energy is better described by

$$V'(z, \theta) = +mgz + \frac{1}{2} k z^2 + \frac{1}{2} \kappa \theta^2 + \varepsilon z \theta \quad , \tag{3}$$

where the term $+mgz$ is the additional gravitational potential energy. The new potential-energy function V'(z, θ) has a non-zero minimum value,

which defines the actual equilibrium condition of the system. That minimum is easily shown to lie at

$$z_{eq} = -mg\kappa\,(k\kappa - \varepsilon^2)^{-1} = -\frac{mg}{k}\{1 - \frac{\varepsilon^2}{k\kappa}\}^{-1} \quad ; \tag{4a}$$

$$\theta_{eq} = +\varepsilon mg(k\kappa - \varepsilon^2)^{-1} = -\frac{\varepsilon}{\kappa} z_{eq} \quad . \tag{4b}$$

These equations show that the spring stretches gravitationally under the weight *mg*, and also that the helical spring unwinds under load to an extent proportional to the coupling constant ε. (These results will provide experimental checks on parameter values in section III and IV.)

Now the actual potential V'(z, θ) can be written in an expansion about the equilibrium position (z_{eq} , θ_{eq}), with the exact result

$$V'(z,\theta) = V_{\min} + 0\,(z - z_{eq}) + 0\,(\theta - \theta_{eq}) + \frac{1}{2}k(z - z_{eq})^2 + \frac{1}{2}\kappa(\theta - \theta_{eq})^2 + \varepsilon\,(z - z_{eq})\,(\theta - \theta_{eq}) \quad . \tag{5}$$

Apart from a constant offset, this V' function happily has the same form as (2) in terms of the departures from equilibrium, so we can hereafter subsume the effects of the gravitational loading of the system by taking the equilibrium positions (4) as defining the zero-values for our coordinates, and then using (2) as our potential-energy expression.

We recognize (5) as a Taylor expansion of the total (elastic plus gravitational) potential energy of the system, in the variables (z - z_{eq}) and (θ - θ_{eq}). The coefficients for the first-order terms are required to be zero

by the definition of equilibrium, and the three terms in second order are the only such terms that can appear. If there were to be higher-order terms in (2), they would also appear in (5); but such terms are *not* relevant to the frequencies of small oscillations in z and θ about their equilibrium values. So the models (5) or (2) are complete for the case of interest.

With kinetic- and potential-energy expressions of the form (1) and (2), it is easy to use the Lagrangian T - V to deduce the equations of motion of the system:

$$m\ddot{z} + k z + \varepsilon\theta = 0 \quad ; \tag{6a}$$

$$I\ddot{\theta} + \varepsilon z + \kappa\theta = 0 \quad . \tag{6b}$$

The simple quadratic form of the potential energy has given very simple, though coupled, equations of motion. These can be solved for normal modes by supposing that both z- and θ-coordinates evolve as simple sinusoids[7],

$$z(t) = A\cos(\omega t) \quad , \tag{7a}$$

$$\theta(t) = \Theta\cos(\omega t) \quad ; \tag{7b}$$

with a common normal-mode frequency ω, and normal-mode amplitudes A and Θ, yet to be found. Inserting these modes into (6) gives the coupled (homogeneous) system of algebraic equations

$$(-m\omega^2 + k)\,A + \varepsilon\,\Theta = 0 \quad ,$$

(8a)

$$\varepsilon\,A + (-I\,\omega^2 + \kappa)\,\Theta = 0 \quad ,$$

(8b)

which has non-trivial solutions only if the determinant of the coefficient matrix vanishes:

$$\begin{vmatrix} k - m\,\omega^2 & \varepsilon \\ \varepsilon & \kappa - I\,\omega^2 \end{vmatrix} = 0 \quad .$$

(9)

Expanding this gives a quadratic equation for ω^2; it can be simplified by defining two 'uncoupled frequencies' which would describe the separate *z*- and θ-motions if ε were to vanish in (6):

$$\omega_z^{\,2} \equiv \frac{k}{m} \quad ; \quad \omega_\theta^{\,2} \equiv \frac{\kappa}{I} \quad .$$

(10)

The equation for the normal-mode frequencies then takes on the form

$$\omega^4 - (\omega_z^{\,2} + \omega_\theta^{\,2})\,\omega^2 + (\omega_z^{\,2}\,\omega_\theta^{\,2} - \frac{\varepsilon^2}{m\,I}) = 0 \quad .$$

(11)

Notice that the *sign* of ε has disappeared here, as only ε^2 affects the frequencies ω. Now solving the quadratic equation (11), we find that the normal-mode frequencies can be written as

$$\omega_\pm^{\,2} = \frac{1}{2}\{(\omega_z^{\,2} + \omega_\theta^{\,2}) \pm \sqrt{(\omega_z^{\,2} - \omega_\theta^{\,2}) + \frac{4\varepsilon^2}{m\,I}}\ \} \quad .$$

(12)

In Section IV the complicated algebraic structure of this result will be rendered much more understandable.

With the 'eigen-frequencies' thus specified, the linear equations in (8) become consistent, and either of them can be used to predict the ratio of amplitudes that must appear in the normal mode. We find that the higher-frequency mode must have

$$\Theta_+ / A_+ = +(\varepsilon / I)\,(\omega_+{}^2 - \omega_\theta{}^2)^{-1} \quad , \tag{13a}$$

while the lower-frequency mode must have

$$\Theta_- / A_- = -(\varepsilon / I)\,(\omega_\theta{}^2 - \omega_-{}^2)^{-1} \quad . \tag{13b}$$

Since both denominators that appear in (13) turn out to be positive, it is worth noting that these predict Θ/A ratios of opposite *sign*, which unambiguously distinguishes the two normal modes from each other.

To illustrate the energy-interchange phenomenon for which the Wilberforce pendulum is famous, it is sufficient to consider a superposition of the form

$$z(t) = A_+ \cos(\omega_+ t) + A_- \cos(\omega_- t) \quad ; \tag{14a}$$

$$\theta(t) = \Theta_+ \cos(\omega_+ t) + \Theta_- \cos(\omega_- t) \quad , \tag{14b}$$

and these equations allow us to understand the ideally-tuned Wilberforce pendulum of the traditional coupled-oscillator demonstrations. If such a pendulum is excited by pulling it down without rotation, followed by a release from rest, we need an initial condition of zero angular deflection; this requires that the constants Θ_+ and Θ_- be equal and opposite. But if we want the vertical translational motion to pass (after an energy-

exchange time) instantaneously through a state of rest, we also need the constants A_+ and A_- to be equal in value. The requirements $\Theta_+ / \Theta_- = -1$ and $A_+ / A_- = +1$, together with (13), entail that

$$-1 = \frac{(\Theta_+ / \Theta_-)}{(A_+ / A_-)} = \frac{\Theta_+ / A_+}{\Theta_- / A_-} = -\frac{\omega_\theta{}^2 - \omega_-}{\omega_+{}^2 - \omega_\theta{}^2} \quad , \tag{15}$$

which can be simplified using (12) to give

$$2\omega_\theta{}^2 = \omega_+{}^2 + \omega_-{}^2 = \omega_z{}^2 + \omega_\theta{}^2, \quad or \quad \omega_z{}^2 = \omega_\theta{}^2 \quad , \quad \frac{k}{m} = \frac{\kappa}{I} \quad . \tag{16}$$

This is the mathematical expression of the condition for 'ideal tuning' of the Wilberforce pendulum, and it says that the frequencies of the (uncoupled) modes have to match. It is usually attained via adjustment of the rotational inertia I of the pendulum bob. But it is crucial to note that *whether or not* the tuning is 'ideal' in this sense, the two normal modes (12, 13) still exist.

The full energy interchange which occurs for ideal tuning defines an energy exchange time T_{ex}, which is related to other measureable parameters. For the conditions imposed on $A_\pm$ and $\Theta_\pm$ above, we have at t=0 all the energy in the translational motion of the system. For the two terms in (14a) to go from in-phase, to fully out-of-phase, motion requires that a phase difference of π radians accumulate in the arguments of the two cosine functions in (14a); this occurs at a time

$$(\omega_+ t - \omega_- t) = \pi \quad , \; ie. \quad t = T_{ex} = \frac{\pi}{\omega_+ - \omega_-} \quad . \tag{17}$$

By this time, the initially out-of-phase cosines in (14b) have come to be fully in phase, which accounts for the motion being entirely rotational at time $t = T_{ex}$. The energy interchange cycle continues in time increments of T_{ex}.

At the ideal-tuning condition (16), it is easy to work out the normal mode compositions (13) to find that

$$\Theta_+ / A_+ = -\Theta_- / A_- = \sqrt{\frac{m}{I}} \quad . \tag{18}$$

If we connect the rotational inertia I to the product of the mass m and the square of a radius of gyration ρ, according to $I \equiv m\,\rho^2$, then the mode compositions are given by the very simple relation

$$\Theta_\pm / A_\pm = \pm\sqrt{\frac{m}{m\rho^2}} = \pm\frac{1}{\rho} \quad , \tag{19}$$

which is a useful guide to setting up the normal modes in the ideal-tuning case.

All the theoretical modeling thus far has entirely neglected any dissipation in the system, and happily this is a good approximation provided that the timescale for energy loss is long compared to the energy-exchange time. In practice, we find that small-amplitude translational oscillations drop to $1/\sqrt{2}$ of their initial size after about 5 minutes $\approx$ 300 s, which gives an energy-decay half-life that's comfortably large compared to the energy exchange time at optimal tuning, which we find to be $T_{ex} \approx 15$ s.

III. Experiment

We took all of the data used in this paper on a commercial Wilberforce pendulum that has been previously discussed[4,5] in this Journal. Its spring is made of 1-mm diameter steel wire, wound in a helix conforming to the threads of a right-handed screw. Appendix A discusses our model for the effective mass m, and the rotational inertia I, of the spring-mass system. The appeal of the apparatus is that I's value can be changed over a wide range with good repeatability (while m is left unchanged) by redistributing parts of the mass of the 'pendulum bob' to differing distances from its axis of rotation.

When we fix the top end of the pendulum's spring, and lower its bob until it comes to rest (both translationally and torsionally), the spring stretches and unwinds relative to those (inaccessible) values which would obtain in zero gravity. Happily the displacements in z and θ predicted by (4) are linear in the suspended mass m, so we can rewrite those equations as

$$\Delta z_{eq} = -\frac{\Delta m\, g}{k}\{1-\frac{\varepsilon^2}{k\kappa}\}^{-1} \quad ; \tag{20a}$$

$$\Delta\theta_{eq} = -\frac{\varepsilon}{\kappa}\Delta z_{eq} \quad . \tag{20b}$$

We achieved a mass change simply by adding temporarily a mass of Δm = 40. g to the bob of the pendulum, and found measured static displacements (with uncertainties)

$$\Delta z_{eq} = -0.145\,(3)\,m \quad ; \Delta\theta_{eq} = +42\,(3)^{\circ} = 0.73\,(5)\,rad \quad . \tag{21}$$

Here we've taken z to be positive upwards, and θ to be positive for counter-clockwise rotation of the bob (as seen from above). We'll show below that the bracketed factor in (20a) is within 1% of unity, so that with ($\Delta m\, g$) a known quantity, these results basically give us the values of k and (ε/κ). Note that the *sign* of ε is determined by these observations; we find that our helical spring 'unwinds' somewhat under load, which for our definition of θ means that $\Delta\theta$ is positive, and thus ε is positive also.

All of the rest of the data in this paper come from dynamically, rather than statically, obtained observations. We describe first a procedure for 'ideal tuning' of a Wilberforce pendulum; next, how to launch it in its normal modes; and last, how to find those normal modes at any other tuning of the pendulum. Our 'tuning parameter' is specified at this stage by the number of full turns, n, of the nuts on the side studs of the pendulum bob, measured from n=0 at their innermost positions. This allows reproducible translations of Δr = 1.00 mm outward for each Δn = 1, since the nuts ride on threaded studs of pitch 1.00 mm.

The goal of 'ideal tuning' is to make possible the display of complete interchange of energy between translational and rotational motion of the bob. We excite our system by pulling the bob straight down (using perhaps z_0 = -0.20 m, and θ_0 = 0 rad) and then releasing it from rest[8]. The earliest oscillations of the system are translational, but energy soon couples into the rotational motion of the bob. There comes a time at which translational motion is minimal, and rotational motion is most

dramatic. The goal for 'ideal tuning' is for this minimum in translational motion to reach all the way down to *zero*. For our system, that condition is achieved for a setting near n = 8 turns outwards for all four tuning nuts.

Of course once this full exchange of translational to rotational energy is achieved, the energy exchanges continue indefinitely, each taking the time T_{ex} of (17). But now it's time to move beyond the standard demonstration to the excitation of normal modes, which (by contrast) display ongoing motion with no energy exchange at all. We find first the normal modes that exist at the ideal-tuning condition, by launching the pendulum from a state of rest at initial conditions such as (z_0 = -0.20 m, $\theta_0 \approx \pm$ 11 rad) which combine translation and rotation.

Time evolution from such initial conditions displays much less 'energy exchange' than the standard demonstration; and for the right (empirically determined) combination of initial conditions Δz_0 and $\Delta\theta_0$, there is no energy interchange at all. The resulting motion is characterized by translational and rotational motions which reach turn-around points that are, and that stay, in synchrony, just as (7) predicts. The motion in $z(t)$ is oscillatory within an envelope which displays no 'beats', but only a slow exponential decay due to damping.

Once a normal mode is recognized, it's worth trying the combination of initial conditions with the opposite *sign* of θ_0, since theory predicts that this will give the *other* normal mode (in the ideal-tuning case). The two normal modes differ both qualitatively and quantitatively. The qualitative

difference corresponds to the sign difference in Θ/A for the two modes; visually, in either normal mode, the pendulum's bob displays a motion akin to that of an auger boring into a solid. But the two normal modes of the Wilberforce pendulum appear to act as augers of *opposite*-handed threading. The quantitative difference between the two normal modes is that their *periods* of oscillation differ. The physical reason is that in one mode, the spring is unwinding as it stretches; in the other mode (the one of shorter period, ie. higher frequency) the spring is becoming more tightly wound as it stretches.

Once a given normal mode can be excited purely, using the correct combination of initial conditions, it can be timed with considerable accuracy merely by eyeball and stopwatch. The data in Table 1 were all obtained by stopwatch timing of 50 full cycles of a normal mode. For our pendulum, typical cycle times are about 2.7 s, so eye-to-hand reaction time can be a small fraction of one cycle. Because the same reaction time applies to the start and the stop of a timing interval, and because reaction times are further diluted over 50 cycles, it becomes possible to measure periods of oscillation to a precision of better than a part in a thousand.

Now the normal modes thus found (and timed) for the ideal-tuning condition also exist for every other setting of the tuning parameter n. The difference is that for each new setting of n, there are new combinations of z_0 and θ_0 which lead to a normal mode. The distinct ratios θ_0/z_0 required for the two normal modes remain of opposite sign, but their magnitudes change systematically, and differently, with the

tuning. Thus it's easiest first to find (and to time) the normal modes with the pendulum tuned not far from the ideal-tuning condition, and then to explore systematically outwards from that point.

In the end, we covered tuning over the full range of n=0 to n=26, by steps of size Δn=2, finding and timing both normal modes for 14 settings of n. As it happened, this gave us tuning over a range not as large as desired. So to explore in the regime of rotational inertia *smaller* that that provided by having all four nuts maximally inwards, we removed two of the nuts from the side studs, and threaded them instead onto the pendulum-bob's *top* stud. Thus we preserved invariant the mass of the bob, but lowered its rotational inertia considerably. The other two nuts, left on the side studs, could still be turned out by n^* turns from their innermost positions. We also found the normal-mode periods for settings of this n^* from n^*=0 to n^*=6, by steps of size $\Delta n^* = 2$.

Those results are listed, in order of increasing rotational inertia I, in Table 1. From the observed timings T_{50} of 50 full cycles of oscillation, we can compute periods $T = T_{50}/50$, frequencies $f = 1/T$, and angular frequencies $\omega = 2\pi f$. We'll see that ω^2-values are of the greatest significance theoretically, and we'll label the higher (vs. the lower) frequency by a subscript + (vs. -) systematically.

The 'ideal tuning' condition does not appear among the listings of Table 1, though we'll see it can be found after-the-fact from the detailed modeling of Section IV. But it occurs near a setting n=7.6, where the two normal modes exhibit T_{50} values near 131.3 and 144.4 s, so the two

periods are near 2.626 and 2.888 s, and the frequencies are about 381 and 346 mHz (milliHertz). The angular frequencies are then ω_+ = 2.393 rad/s and ω_- = 2.176 rad/s. The predicted energy-exchange time (17) at the ideally-tuned condition is then

$$T_{ex} = \pi/(\omega_+ - \omega_-) = \pi/(2.393 - 2.176)\, s^{-1} = 14.5\, s \quad , \tag{22}$$

and this matches adequately the energy exchange times that can be observed after a launch from initial conditions such as (z_0 = -0.20 m, θ_0 = 0). Recall that our definition of T_{ex} gives the time for *one*-way energy transfer, so that 2 T_{ex} = 29. s predicts the time interval between successive occurrences of (say) the absence of rotational motion.

But the real motivation for taking all the data in Table 1 is that a *much* more detailed analysis can be accomplished using the whole of this set of rather precisely-determined information. To do so, we'll see that we need a model which translates the raw independent variable (turns count *n* or *n** for the tuning nuts) to the dynamically-relevant variable, the rotational inertia I of the pendulum bob. This could be done by a variety of means, but in Appendix A we show how that modeling can be accomplished using only the masses and dimensions of components of the pendulum bob. The results are listed in columns in Table 1, first as I-values in the suitable units of g mm^2, and then as the important (1/I)-values, converted into standard units of (kg m^2)$^{-1}$.

IV. Analysis

The data thus obtained for normal-mode periods can be compared to the theoretical predictions for coupled oscillators, (12), in several ways. We embark here on a sequence of graphs which successively tease out parts of the theoretical model, and give very direct ways to form initial estimates of the parameters of the model. The graphs depend on forming artful combinations of the *squares* of the observable angular frequencies ω_+ and ω_-. Since those squares of the normal-mode frequencies, ω_+^2 and ω_-^2, define the roots of the quadratic equation (11), it follows that this equation can also be written in factorized form as

$$0 = (\omega^2 - \omega_+^{\,2})(\omega^2 - \omega_-^{\,2}) = \omega^4 - (\omega_+^{\,2} + \omega_-^{\,2})\omega^2 + (\omega_+^{\,2}\omega_-^{\,2}) \quad . \tag{23}$$

Comparing this form with (11) makes it clear (as computation using (12) will confirm) that the sum, and the product, of the roots ω_+^2 and ω_-^2 take on quite simple forms, and forms very well suited to plotting of empirically-obtained data.

For a first example, we find by comparing (11) and (23) that

$$\Sigma \equiv \omega_+^{\,2} + \omega_-^{\,2} = \omega_z^{\,2} + \omega_\theta^{\,2} = (k/m) + \kappa(1/I) \quad . \tag{24}$$

Since the sum of squares of mode frequencies Σ can be computed directly from observable quantities, this equation motivates a plot of observed ($\omega_+^2 + \omega_-^2$) values as a function of the independent variable ($1/I$). Note that the sum Σ, plotted as (24) suggests, is predicted to be *in*dependent of the value of the coupling parameter, ε. The results, computed using

the mode periods listed in Table 1, and the inertia calculations of Appendix A, are plotted in Fig. 1. The points do indeed lie on a line as predicted by (24), and the intercept and slope respectively give initial estimates of the parameters

$$k/m = 5.215\, s^{-2} \quad ; \tag{25a}$$

$$\kappa = 8.35 \times 10^{-4}\, N.m \quad ' \tag{25b}$$

with uncertainties of order 0.3% (but to be addressed in more detail below).

For a second example of parameter extraction, we find from (11) and (23) an expression for the *product* of the squares of the normal-mode angular frequencies:

$$\Pi \equiv \omega_+^{\,2}\, \omega_-^{\,2} = \omega_z^{\,2}\, \omega_\theta^{\,2} - \frac{\varepsilon^2}{mI} = (\kappa \frac{k}{m} - \frac{\varepsilon^2}{m})(1/I). \tag{26}$$

Again this motivates a plot of an experimentally observable dependent variable as a function of the independent variable, the well-modeled ($1/I$) values. The results, again using Table 1 and Appendix A, are plotted in Fig. 2. Here too the points lie along a line, and this time a line passing very nearly through the origin, as (26) in fact predicts. The best-fit line shown in Fig. 2 extrapolates to an $\underline{x}$-axis intercept of +17 $(\text{kg m}^2)^{-1}$, a departure from zero of at most 1.5-σ statistical significance, and in any case very small indeed compared to x-axis data values ranging from 3800 to 8800 $(\text{kg m}^2)^{-1}$. The discrepancy, if real, points perhaps to a systematic error, of size well under 1%, in the rotational-inertia model of

Appendix A. We also get from Fig. 2 a slope of value 4327 x 10^{-6} N.m/s^2. Since from (26) this quantity is also given by

$$(k/m)\,\kappa\,\{1-\frac{\varepsilon^2}{k\kappa}\}\quad , \tag{27}$$

and since ε^2 turns out to be so small compared to $(k\,\kappa)$, (25) and (26) together provide a method of finding ε^2 of rather poor sensitivity. Using instead the value 0.9911 found below for the bracketed quantity in (27), we instead deduce from Fig. 2's slope the estimate

$$(k/m)\kappa = 4366\times 10^{-6} N.m/s^2, \tag{28}$$

which compares neatly to the result 4354 x 10^{-6} N.m/s^2 deduced from (25).

Finally, since $(\omega_+^2 + \omega_-^2)$ and $(\omega_+^2\,\omega_-^2)$ both have rather simple forms, the additional observable quantity $(\omega_+^2 - \omega_-^2)^2$ also has a form much simpler than (12), from which it can be shown that

$$\Delta^2 \equiv (\omega_+^2 - \omega_-^2)^2 = (\omega_z^2 - \omega_\theta^2)^2 + \frac{4\varepsilon^2}{mI}$$
$$= (\frac{k}{m})^2 + (-2\frac{k}{m}\kappa + 4\frac{\varepsilon^2}{m})\,(1/I) + \kappa^2\,(1/I)^2 \quad . \tag{29}$$

Again plotting experimentally-determined values of the left-hand side as a function of the $(1/I)$ values emerging from our inertia model, we are led by (29) to expect a parabolic dependence. The data are shown in Fig. 3, and a parabola indeed appears. The precision of the experimental values of ω_+^2 and ω_-^2 is high enough that, even after the differencing operation of (29), the points in Fig. 3 show scarcely visible scatter about the parabola.

A parabola of the form $c_0 + c_1(1/I) + c_2\,(1/I)^2$ could be fit to the data of Fig. 3, but we choose instead to emphasize the location of the minimum by using as fitting function the parabolic form

$$\Delta^2 = A\,(1/I - B)^2 + C \quad , \tag{30}$$

so that the parabola's minimum is located on the horizontal axis at $(1/I)$-value B, where the function reaches its smallest value of C. Now Δ^2 in (29) can also be transformed into a parabolic dependence on argument $(1/I)$ around its minimum, with results

$$A = \kappa^2 \quad , \tag{31a}$$

$$B = \frac{k/m}{\kappa}\,\{1 - 2\frac{\varepsilon^2}{k\kappa}\} \quad , \tag{31b}$$

$$C = 4\frac{\varepsilon^2}{m}\,\frac{k/m}{\kappa}\,\{1 - \frac{\varepsilon^2}{k\kappa}\} \quad ; \tag{31c}$$

so it becomes possible to compare the results of the parabolic fit in Fig. 3 to the parameters in the model. From (31a) and the value A = 702.3 x 10^{-9} $(\text{N.m})^2$ from the fit, we find

$$\kappa^2 = 702.3\times10^{-9}(N.m)^2\ ,\ or\ \ \kappa = 8.38\times10^{-4}\,N.m \quad , \tag{32a}$$

which comports very neatly with (25b) above. From (31b), using the value B = 6171 $(\text{kg m}^2)^{-1}$ from the fit, and the value $\{1 - 2\,\varepsilon^2/(k\kappa)\}$ = 0.9821 deduced below, we find

$$(k/m)/\kappa = 6283\,(kg\,m^2)^{-1}$$

(32b)

which compares with the value 6246 (kg m^2)$^{-1}$ deduced from (25) above. Finally, we see from (31c) a result that depends strongly on the parameter (ε^2/m), and connects it to the value C = 0.954 s^{-1} from the quadratic fit. Solving, we find

$$\varepsilon^2/m = 38.3\times10^{-6}\,N^2/kg \quad .$$

(32c)

In fact the height of the parabola's minimum above zero is determined directly by the value of ε^2/m, so the C-parameter of the parabolic fit provides a rather high sensitivity to its value. We'll show next that this small coupling constant can be determined, by a global fitting of the complete data set, to a precision better than 1% of its value.

The three distinct fits thus far have provided visually-appealing graphs, and a variety of estimates for three parameters which fully describe the theoretical 'spectroscopy' of the system: k/m, κ, and ε^2/m. But thus far it's not clear what the 'best estimates' for those parameters are, nor what their actual uncertainties are. We address this problem by making a global fit of the entire data set to a three-parameter model, treating the modeled ($1/I$) values as the independent variable, and treating ω_+^2 and ω_-^2 as two functions dependent upon it. Then we define a global χ^2 'misfit function' between data and theory by

$$\chi^2 = \sum_{j=1}^{18} \frac{1}{\sigma^2}\,[\,d^{(+)}{}_j - \omega_+{}^2(1/I_j)\,]^2 + \sum_{k=1}^{18} \frac{1}{\sigma^2}\,[\,d^{(-)}{}_k - \omega_-{}^2(1/I_k)\,]^2$$

(33)

where σ is an assumed numerical uncertainty for each experimental ω^2-value, and where the fitting functions which ought to match the data are given by a version of (12),

$$\omega_{\pm}{}^2(1/I;\ k/m,\ \kappa,\ \varepsilon^2/m) = \frac{1}{2}\{\ (\frac{k}{m} + \kappa\frac{1}{I}) \pm \sqrt{(\frac{k}{m} - \kappa\frac{1}{I})^2 + \frac{4\varepsilon^2}{m}\frac{1}{I}}\ \}\quad . \tag{34}$$

The global χ^2 sum includes all 36 data points, 18 $d_i^{(+)}$ data values of ω^2 for the upper-frequency modes, and 18 more $d_j^{(-)}$ values for the lower-frequency modes, and it can be minimized as a function of its three arguments, the three fitting parameters. The minimum value of χ^2 ought to come out near 36-3 = 33 if the assumed input uncertainty σ is properly chosen, and if the data and the model do not differ systematically. To get an estimate for the input uncertainties, we start with the period values of Table 1, with typical numbers for 50**T* of 140 s, with uncertainties estimated near 0.07 s. This gives fractional uncertainties $\delta T/T$ near 1/2000, and thus $\delta\omega^2/\omega^2$ near 1/1000. Since typical numerical values of ω^2 are near 5 s^{-2}, we provisionally assign σ to be 1/1000 of this, or 0.005 s^{-2}. Using this gives a χ^2 sum whose minimum is larger than the expected value of 33, so we conclude *a posteriori* that a better estimate for σ is 0.0078 s^{-2}, to be attached to each ω^2-value. This enlarged uncertainty may be an indication of larger-than-expected observational errors, or of small systematic errors in the inertia model of Appendix A.

The parameter values which minimize χ^2 are

$$k/m = 5.229(2)\ s^{-2} \quad ;$$

(35a)

$$\kappa = 8.327(4) \times 10^{-4}\ N.m \quad ;$$

(35b)

$$\varepsilon^2/m = 38.8(3) \times 10^{-6}\ N^2/kg \quad ;$$

(35c)

where the uncertainties apply to the last digit shown. They are assigned on the '$\chi^2 + 1$' basis, and they reflect the *a posteriori* assignment of σ discussed above. Because the data span an adequately large range of ($1/I$) values, the parameters' values turn out to be very nearly uncorrelated. The numbers can also be used to establish

$$\{1 - \frac{\varepsilon^2}{k\kappa}\} = \{1 - \frac{\varepsilon^2/m}{(k/m)\kappa}\} = 0.9911 \quad ,$$

(36)

whose nearness to one is a good dimensionless measure of the weakness of the coupling, and whose value has been used above. Together with the value of m = 0.5200 kg from Appendix A, the values (35) also allow the extraction of

$$k = 2.719\ (1)\ N/m \quad ;$$

(37a)

$$\varepsilon = (+)0.00449\ (2)\ N \quad ;$$

(37b)

$$\varepsilon/\kappa = 5.39\ (3)\ m^{-1} \quad .$$

(37c)

The uncertainties in (35) give a good description of statistical uncertainties in the data, but there may still be systematic errors in the

parameters' values. In particular, any systematic errors in the inertia model of Appendix A will show up creating systematic errors in the parameters above, in particular affecting the value assigned to the torsion constant κ. There are additional errors possible in (k/m), since the theory assumes the top end of the spring is fixed, but in the experiment it was attached to a spring mount slightly compliant in the z-direction. (This made possible the sensing, or the driving, of the vertical translational motion of the system.) Nevertheless, the values in (35) do show how tightly can be constrained the parameters of a model intended to describe the observable 'spectroscopic' features of the Wilberforce pendulum.

Another use of the constants deduced above is to evaluate the location of the 'ideal tuning' condition (16). We see that this requires

$$1/I = (k/m)/\kappa = 6280\ (kg\ m^2)^{-1} \quad , \tag{38}$$

with an uncertainty of order 0.06%, or ±4 (kg m^2)$^{-1}$. Inverting the model of Appendix A, we see that this occurs for turns-count n = 7.59 ± 0.02 turns. Another use of these constants is to evaluate the radius of gyration ρ in (19), which gives ρ = (17.5 ± 0.1) mm [9], and from that, the ideal-tuning mode composition ratio, Θ/A = 57 m^{-1}. This is equivalent to requiring, in the ideal-tuning case, an initial vertical displacement of z_0 = -0.11 m for initial rotational displacements of $\theta_0 = \pm 2\pi$, ie. for ±1 full rotations, of the bob.

The parameters (35) can also be used to evaluate the theoretical expressions for the mode frequencies (34), and to give the limiting values

they would take on in the case that $\varepsilon \to 0$. These theoretical expressions, together with the experimental data, are plotted as functions of the inverse rotational inertia, $(1/I)$, in Fig. 4. The data and the model illustrate vividly an 'avoided crossing', as they both vary with $(1/I)$ in curves that are asymptotic toward the uncoupled-modes predictions, but depart from them characteristically given the presence of even the weak coupling between the modes. Given the close visual agreement between the data, and the model for it, the detailed comparison between the two is best conducted in terms of the residuals, or (data - model) values, plotted as functions of $(1/I)$; doing so reveals the expected scatter on the order of $\pm 2\sigma$, but no systematic structure.

The curves in Fig. 4 also give a fine way to understand interactively the role of the three parameters in the theory. In particular, the combination (k/m) gives the height of the horizontal asymptote, and κ gives the slope of the tilted asymptote. The coupling constant (ε^2/m) then gives the degree to which the curves depart from the lines toward which they are asymptotic.

We thus regard the three parameters (35) as a satisfactory description of the dynamically-observed properties of the Wilberforce pendulum. As a final 'reality check' of lower precision but wholly independent origin, we turn to the static deformation values (21), which were obtained by adding a mass $\Delta m = 40.$ g, or a load $(\Delta m\, g) = 0.392$ N, to the pendulum bob. Using the value (36) established above, we deduce from them the values

$$k = -(0.392\ N)\,(0.9911)^{-1} / (-0.145\ m) = 2.73\ N/m \tag{39a}$$

$$\varepsilon/\kappa = -\Delta\theta_{eq} / \Delta z_{eq} = -(0.73\ rad)/(-0.145\ m) = +5.0\ m^{-1} \tag{39b}$$

The first of these gives a value of k with an uncertainty of about ±0.06 N/m, and in satisfactory agreement with (37a). The second of these establishes that the sign of ε is positive. The value it gives for ε/κ has an uncertainty of about ±0.3 m^{-1}, and it is in fair agreement with (37c). We conclude that the 'static data' give results less precise than the dynamic methods, but consistent with them.

Yet another use of these parameters is to obtain 'retrodictions' of the compositions of the two normal modes, as a function of the inverse rotational inertia and hence of the turns-count, n. We use the results (13), and plot them as a function of $(1/I)$ values, using the parameters of (35) to evaluate the model's predictions. The result are presented as a graph of (Θ_+/A_+) and (Θ_-/A_-) in Fig. 5. Both ratios of 'required rotation per unit translation' reach a magnitude of $1/\rho$ = 57 rad/m at the 'ideal tuning' value of $(1/I)$ = 6280 (kg m^2)$^{-1}$, but of course with opposite sign. The curves of $(\Theta_\pm/A_\pm)$ display *first*-order sensitivity to departures from the ideal-tuning condition, so that if the proportions (Θ/A) for both normal modes can be measured, this provides a quite sensitive test of the location of the ideal-tuning condition.

For the rather large de-tunings accomplished in the experiments above, of course, the mode compositions change markedly: the initial condition of rotation per unit translation required for launching a normal mode

changes, upwards and downwards, by about a factor of *five* at the extremes of the (1/I) values we've used. It follows that the appearance of the normal modes changes dramatically away from ideal tuning; there are two limits of normal modes which are chiefly translational, and two other limits of normal modes which are chiefly rotational, in character. Another way to see this change of character is to analyze the kinetic-energy content of the oscillating normal modes. According to (7), there are two instants in each cycle at which $z = 0 = \theta$; at these times, the energy of the system is wholly kinetic in character. Using (7) for computing the relevant velocities, it is easy to get an expression for the fraction f_{trans} of the kinetic energy that is due to translation (as opposed to rotation) at these instants. [Of course (1 - f_{trans}) gives the fraction of energy in rotation.] That fraction is given by

$$f_{trans} = \frac{1}{1 + (\frac{I}{m})(\frac{\Theta}{A})^2} \quad , \tag{40}$$

and this expression can be evaluated, and plotted, for both of the normal modes, as a function of (1/I) over the range of interest, using the parameters (35) to evaluate the theoretical expressions (13). The results are shown in Fig. 6, and again they display special results at the ideal-tuning condition, where the kinetic energy is divided equally between translation and rotation. But at the extremes of the tuning range we've covered, the proportions of kinetic energy, translational:rotational, vary from about 97:3 to 6:94, again illustrating how the normal-mode compositions change dramatically in passing through the 'crossing' region.

V. Conclusions

We conclude that the 'spectroscopy' of the Wilberforce pendulum confirms, in detail and with high precision, the theoretical treatment of coupled-oscillator phenomena. In particular, we find that oscillation frequencies can be measured, and modeled, to precisions of order 0.1%, by rather simple means. Details of the frequencies of the normal modes, in particular their variation with rotational inertia, can be investigated by graphing artful combinations of experimentally observable quantities. The theoretical models turn out to depend on the rotational inertia (as an independent variable), and three theoretical parameters which can be extracted with good confidence and high precision.

The implications of this work extend far beyond the interesting case of the Wilberforce pendulum. *Any* classical system of two harmonic oscillators, coupled by a product-term akin to that in (2), will have an algebra isomorphic to that worked out here. Since any such system will have two normal modes, we conclude that the combinations $(\omega_+^2 + \omega_-^2)$, $(\omega_+^2\ \omega_-^2)$, and $(\omega_+^2 - \omega_-^2)^2$ will also be useful in the analysis of properties of a generic two-coupled-oscillator system. If, in such a system, one inertia-like parameter or force-constant can be varied, we further expect that the normal-mode frequencies ω_+^2 and ω_-^2 will show a characteristic variation with that parameter. In particular, the coupled system ought to display an 'avoided crossing' as a function of the adjustable parameter. The degree of avoidance of the two ω^2-curves (which would have crossed in the absence of coupling) is a sensitive measure of the strength of the coupling that is present.

There is also the exciting possibility of *real-time* variation of such a tuning parameter that gives rise to the possibility of 'adiabatic transfer'[10]. Though this can occur in any system of two coupled oscillators, we'll discuss it here in the language of the Wilberforce pendulum. We imagine a pendulum bob, then, in which (by some internal mechanism) the rotational inertia I can change autonomously and continuously, at a modest rate, while the pendulum is itself oscillating. To use the language of Fig. 4, we imagine a 'bob' of fixed mass, but of rotational inertia that could vary, so that $(1/I)$ changed from (say) 4000 to 9000 $(\text{kg m}^2)^{-1}$ over a few minutes' time.

Suppose, then, that I started large, ie. that $(1/I)$ started small, and further that a Wilberforce pendulum were set up in a chiefly-translational normal mode at the starting value of low $(1/I)$. In the language of Fig. 4, the system would be 'at' point A. Now suppose that I decreased systematically, raising $(1/I)$ from its low to its high value, on a time scale long enough compared to energy-exchange time T_{ex}, but shorter than the energy-decay timescale of the system. 'Adiabatic passage' predicts that the state of the system would 'ride the curve' in Fig. 4, staying in a normal mode (but one of ever-changing composition) as the system passed through states labeled B and C, and ending in the state labeled D. The drama of the outcome is that state D represents a pendulum in a normal mode which is almost purely *rotational* in character. In brief, a continuous, and slow enough, variation in a single parameter would cause an energy transfer from nearly pure translation to nearly pure rotation.

Clearly, the same means, but with a different starting condition, could alternatively be used to 'ride along' the lower curve in Fig. 4; such adiabatic transfers would work for either direction of parameter variation, as well. Unlike the cyclic energy transfers which occur in time T_{ex} for the ideally-tuned Wilberforce system, these adiabatic transfers act to create a one-way transfer of energy which is complete, and which (for a slow enough variation of the system's parameters) does *not* require any careful tuning, timing, or synchronization.

It is not clear if anyone has ever built a Wilberforce pendulum which was designed to exhibit this behavior, though it's possible that such phenomena have been observed accidentally. For such a demonstration to be convincing, it would be necessary to build a shape-changing structure whose mass stayed fixed, whose rotational inertia varied (through the right region) by about a factor of two, and which acted at every stage enough like a rigid body that the system's dissipation would remain small. It would be especially dramatic to build a system in which the tuning parameter could vary continuously but not merely monotonically, making possible a 'trip' such as ABCBA, or even ABCBCD, through the configurations of the coupled-oscillator system.

Such adiabatic transfers are perhaps fanciful exhibits in classical systems, but they are subjects of active research in parallel cases in quantum mechanics[11]. There are plenty of examples of two quantum-mechanical eigenstates whose energy eigenvalues are involved in an avoided crossing; in atomic physics the tuning parameter might be magnetic-field strength, while in molecular physics it might be inter-nuclear separation. In such

cases, the strength of interaction will again manifest itself in the degree of avoidance at the (avoided) crossing. Again, modeling the spectroscopy of the system can provide the values of a set of constants which characterize the interacting states. Even the algebra of the energy values can be very similar to that discussed here, since the eigenvalues will emerge from a determinant such as (9). One chief difference is that in quantum-mechanical cases, it is ω-values, not ω^2-values, which are involved in the algebra. This distinction can be traced ultimately to the fact that the time-dependent Schrödinger Equation is first-order in time, whereas Newton's Second Law leads to classical equations which are second order in time.

Acknowledgements: We thank Zach Smith for his work, and initial data, on this Wilberforce pendulum.

Appendix A: Modeling the rotational inertia of the bob

The purpose of this appendix is to connect the turns count n (or n^*) of the tuning nuts to the rotational inertia I of the pendulum in the Wilberforce system, by using measured values for masses and dimensions of the components.

We start with the measured mass m_s = 78.0 g of the spring itself, and the total mass m_b = 493.7 g of the entire 'bob' of the pendulum. The effective mass of the system for low-frequency translational modes requires the addition of part of m_s to m_b; the simplest model for 'part of' gives the coefficient (1/3), but using Ref. 12, Berg and Marshall[5] show that 0.337 is the better estimate, so we take

$$m = m_b + (0.337)\, m_s = 520.0 \text{ g}.$$

We now work on rotational inertia. The spring, modeled as a thin-walled cylinder of radius r_s = 15.5 mm, would contribute rotational inertia $m_s\, r_s^2$ if it rotated as a rigid cylinder. For the low-frequency torsional modes of the system, we similarly take (0.337) of this as a first contribution to I:

$$I_{spr} = (0.337)\, m_s\, r_s^2 = 6315 \text{ g mm}^2.$$

The 'bob' of the system includes a top nut, a top washer, and a top stud. These together contribute an estimated

$$I_{top} = 71 \text{ g mm}^2$$

to the total I, and they also constitute a net 5.8 g of the rotor's mass. That rotor also includes four tuning nuts, each of measured mass 17.4 g, and four side studs, each of estimated mass 5.55 g. Subtracting all these

leaves a mass of 493.7 - 5.8 - 4(17.4 + 5.55) = m_{main} = 396.1 g for the rotor's cylindrical body proper, which is of radius r_{main} = 17.5 mm. So we get for the solid cylinder an inertia contribution

$$I_{main} = (1/2)\, m_{main}\, r_{main}^2 = 60{,}653 \text{ g mm}^2 .$$

The four side studs can each be modeled as a solid cylinder, of length l = 30. mm and radius 2.75 mm, and (if rotated about their centers of mass) each would contribute $I_{cm} = m\,[(1/12)\, l^2 + (1/4)\, r^2)\,] = 427$ g mm^2. But in fact their centers are off-axis by (17.5 + 15.) mm, giving by the parallel-axis theorem a contribution

$$I_{stud} = I_{cm} + (5.55 \text{ g})(32.5 \text{ mm})^2 = 6289 \text{ g mm}^2.$$

Counting all the pieces thus far, which together give the part of I independent of the four tuning nuts' locations, we reach

$$I_{rigid} = (6315 + 71 + 60{,}653 + 4*6289) \text{ g mm}^2 = 92{,}195 \text{ g mm}^2.$$

To this needs to be added the contributions of the tuning nuts; each has mass m_n = 17.4 g, and has dimensions thickness d = 4.8 mm, outer radius r_2 = 12.0 mm, and inner radius r_1 = 2.75 mm. Rotated about a diameter passing through its center of mass, a nut would give

$$I_{cm} = m_n\,[(1/12)\, d^2 + (1/4)(r_1^2 + r_2^2)] = 692.7 \text{ g mm}^2.$$

But of course the nuts are out on the studs, distant by $r = r(n)$ from the rotation axis. For our rotor, the n=0 value of the turns-count puts the centers-of-mass of the nuts at r_0 = 22.8 mm from the axis, and the 1-mm pitch of the studs ensures that $r(n) = r_0 + n$(1.00 mm) under tuning. So the model for each nut becomes

$$I_{nut} = I_{cm} + m_n\,[r(n)]^2 = [692.7 + 17.4(22.8 + n)^2] \text{ g mm}^2.$$

So for the whole system, when four nuts are each n turns outward of their n=0 positions, we have

$$I(n)/[\text{g mm}^2] = 92{,}195 + 4\,[692.7 + 17.4\,(22.8 + n)^2\,] .$$

If only two nuts are on the studs, the model changes; in this case, the bracketed terms above need a coefficient of 2 rather than 4. But the two nuts mounted onto the top stud each contribute an inertia

$$I'_{\text{nut}} = (1/2)\, m_n\, (r_1^2 + r_2^2) = 1318.6 \text{ g mm}^2 ,$$

so the model in this case becomes

$$I(n^*)/[\text{g mm}^2] = 92{,}195 + 2*1318.6 + 2\,[692.7 + 17.4\,(22.8 + n^*)^2\,] .$$

These results are used in constructing Table 1. Naturally the results for I could be obtained by other means, including direct experimental determination. Even a one- or two-point experimental check, perhaps of $I(n=0)$ and $I(n=20)$, would be a valuable test of the wholly-computed inertia model used here. Such a check might be performed on a separate torsional apparatus, itself equipped with a single torsion fiber, using some simply shaped objects of known mass and easily-computed rotational inertia to calibrate the torsion fiber. Since oscillation-period techniques could be used to sense $I(n)$, precisions of perhaps one part per thousand might be attained. The all-computed models here, by contrast, might contain systematic errors in some of their coefficients of order 1%.

References

1. L. R. Wilberforce, "On the vibrations of a loaded spiral spring", Philos. Mag. **38**, 386-392 (1894).

2. Arnold Sommerfeld, *Mechanics of Deformable Bodies: Lectures on Theoretical Physics* (Academic, New York, 1920), vol. II, pp. 308-314.

3. Ronald Geballe, "Statics and Dynamics of a Helical Spring", Am. J. Phys. **26**, 287-290 (1957).

4. Ulrich Köpf, "Wilberforce's pendulum revisited', Am. J. Phys. **58**, 833-837 (1990).

5. Richard E. Berg and Todd S. Marshall, "Wilberforce pendulum oscillations and normal modes", Am. J. Phys. **59**, 32-38 (1991).

6. Our pendulum was manufactured by Leybold-Heraeus Gmbh, as their model #346 51, in about 1979.

7. Notice that the success of this ansatz implies that the translational and rotational motions are either in phase (if Θ/A is positive), or 180° out of phase (if Θ/A is negative), in any normal mode.

8. This sort of abrupt release will also excite longitudinal-wave modes in the spring, which have higher frequencies (2-3 Hz and above, in our

case) and also more rapid damping. Happily these modes are invisible to eyeball-and-stopwatch timing.

9. It is no accident that at 'ideal tuning', the radius of gyration (17.5 mm) is just a bit bigger than the radius of the turns of the helical spring (15.5 mm). In the limit of a spring of small pitch, the ratio of these numbers is expected to be $(1+\nu)^{1/2}$, where ν is Poisson's ratio ($\approx$0.23) for the spring material. See Eqn. (46) of Ref. 5.

10. There's a tutorial article on the related concept of 'adiabatic invariance' in Frank S. Crawford, "Elementary examples of adiabatic invariance", Am. J. Phys. **58**, 337-344 (1990); a recent article covers 'rapid adiabatic passage' in B. W. Shore et al., "Simple mechanical analogs of rapid adiabatic passage in atomic physics", Am. J. Phys. **77**, 1183-1194 (2009).

11. For a look at avoided crossings in atoms as a function of magnetic-field strength, see Stephan Dürr et al., "Observation of Molecules Produced from a Bose-Einstein Condensate", Phys. Rev. Letters **92**, 020406 (2004). For a review on the process of STIRAP (stimulated Raman adiabatic passage), see K. Bergmann, H. Theuer, and B. W. Shore, "Coherent population transfer among quantum states of atoms and molecules", Rev. Mod. Phys. **70**, 1003-1025 (1998).

12. T. W. Edwards and R. A. Hultsch, "Mass distribution and frequencies of a vertical spring", Am. J. Phys. **40**, 445-449 (1972).

Table 1

Data obtained for normal-mode periods of the Wilberforce pendulum. The 'turns count' gives the tuning parameter, in full turns n (or n^*) of the four (or two) tuning nuts, while the T_{50} values are the measured times required for 50 cycles of oscillation of each normal mode. The model I and $(1/I)$ values come from Appendix A on the rotational inertia of the system.

turns count	T_{50}, in s (faster)	T_{50}, in s (slower)	model I in g mm^2	model $(1/I)$ in (kg m^2)$^{-1}$
$n^* = 0$	115.26 s	139.59 s	114,308	8748
2	116.59	139.59	117,621	8502
4	118.34	139.65	121,212	8250
6	119.98	139.90	125,082	7995
$n = 0$	122.46	140.45	131,147	7625
2	125.17	140.93	137,773	7258
4	127.59	141.78	144,955	6899
6	129.90	142.87	152,695	6549
8	131.67	144.74	160,991	6212
10	133.14	147.13	169,844	5888
12	134.27	149.95	179,254	5579
14	134.87	153.16	189,221	5285
16	135.17	157.01	199,744	5006
18	135.62	160.79	210,825	4743
20	136.08	164.86	222,462	4495
22	136.09	169.15	234,656	4262
24	136.26	173.57	247,407	4042
26	136.56	178.18	260,714	3836

Figure Captions

Fig. 1.

Plotting the sum of the squares of the two angular frequencies, ($\omega_+^2 + \omega_-^2$), derived from the observed periods of the normal modes, as a function of independent variable ($1/I$), the inverse of the modeled rotational inertia. The rms departure of the points from the straight-line fit is about 0.010 s^{-2}.

Fig. 2.

Plotting the product of the squares of the two angular frequencies, ($\omega_+^2\ \omega_-^2$), derived from the observed periods of the normal modes, as a function of independent variable ($1/I$), the inverse of the modeled rotational inertia. The rms departure of the points from the straight-line fit is about 0.052 s^{-4}. Theory predicts that the data fit a straight line with y-intercept *zero*.

Fig. 3.

Plotting the square of the difference of the squares of the two angular frequencies, $(\omega_+^2 - \omega_-^2)^2$, derived from the observed periods of the normal modes, as a function of independent variable ($1/I$), the inverse of the modeled rotational inertia. The rms departure of the points from the parabolic fit is about 0.032 s^{-4}.

Fig. 4.

Observational data, and theoretical models, for the squares of the angular frequencies of the two normal modes of a Wilberforce pendulum, plotted as a function of the inverse of the modeled rotational inertia. The plotted data points come from the measured periods in Table 1, and the independent variable is the inverse of the rotational inertia, as modeled in Appendix A. The curves are plots of the theory (34), evaluated using the three best-fit parameters that describe the system; the straight lines show the results expected in the zero-coupling limit. The rms departure of the data points from the theoretical curves is about 0.008 s^{-2}, or about one-eighth of the size of the plotting symbols used.

Fig. 5.

Theoretical predictions for the mode composition ratio, Θ/A, of (13), evaluated using the best-fit parameters (35), displayed for both normal modes. The two curves both reach magnitude 57 rad/m at the 'ideal tuning' value of $(1/I) = 6280$ $(\text{kg m}^2)^{-1}$.

Fig. 6.

The fraction of the kinetic energy predicted to be in translational motion, computed using (40) and the best-fit parameters (35), and displayed for both normal modes as a function of inverse inertia $(1/I)$.

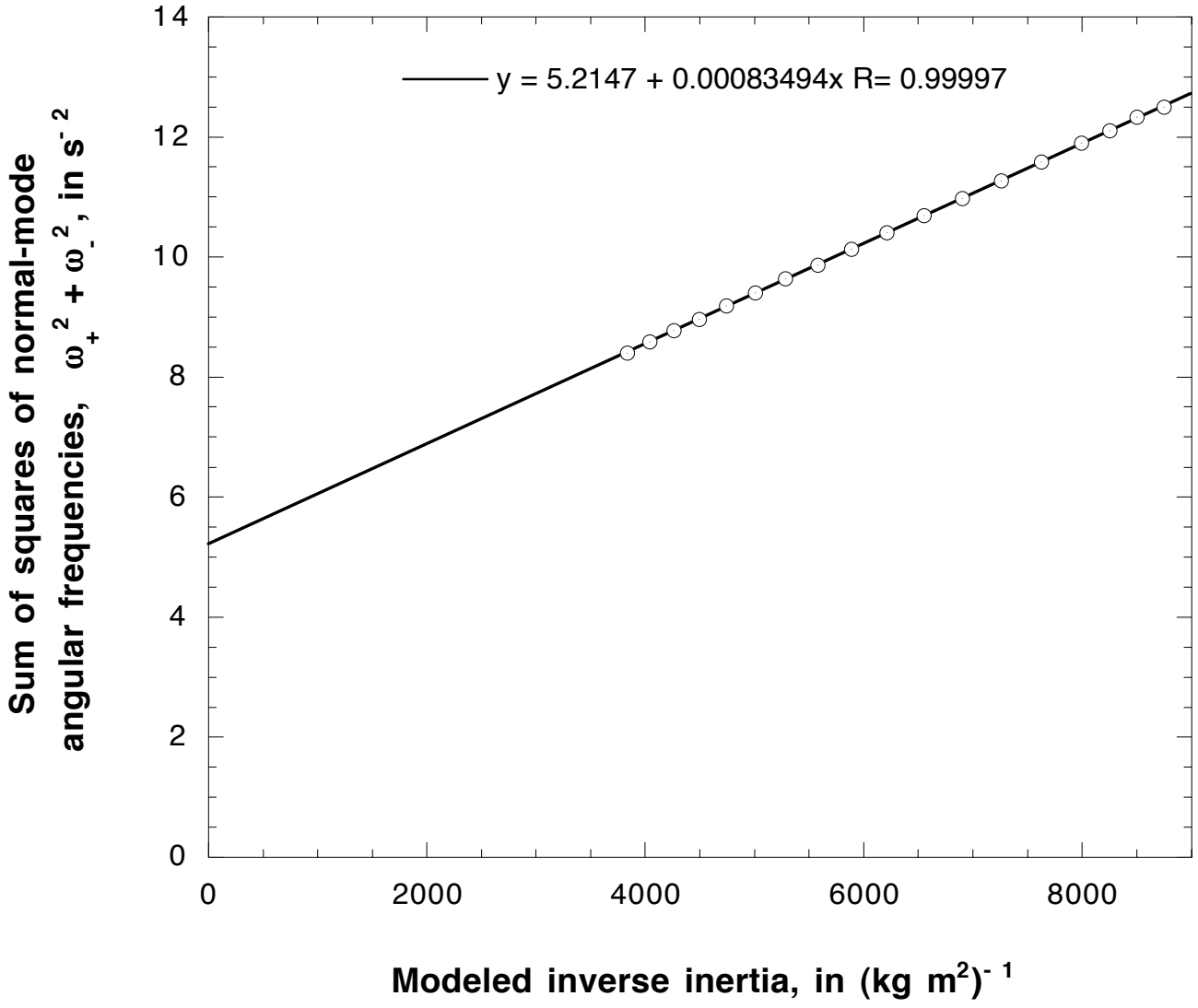
y = 5.2147 + 0.00083494x R= 0.99997
Sum of squares of normal-mode angular frequencies, $\omega_+^2 + \omega_-^2$, in s^{-2}
Modeled inverse inertia, in $(kg\ m^2)^{-1}$
0
2
4
6
8
10
12
14
0
2000
4000
6000
8000

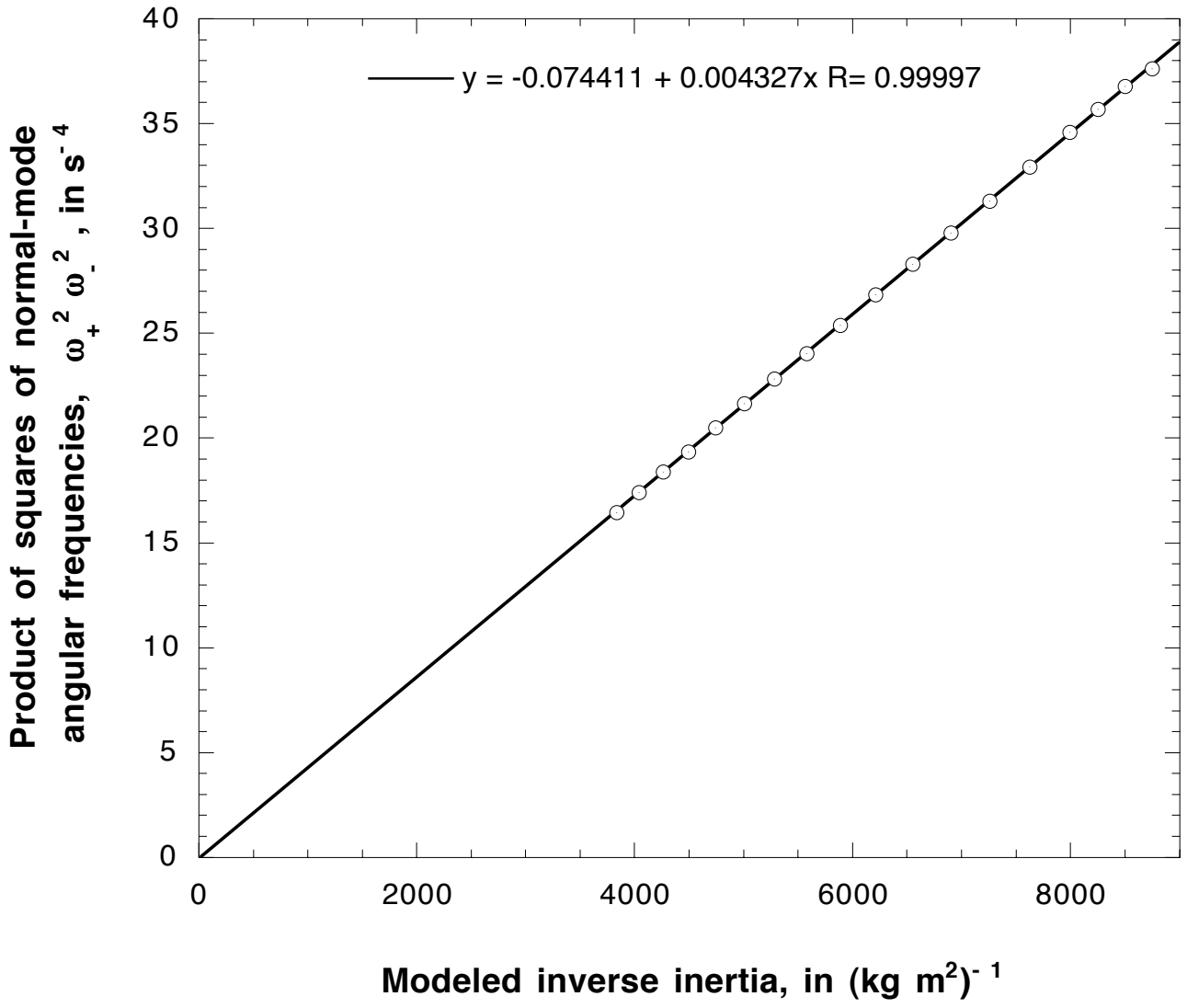
y = -0.074411 + 0.004327x R= 0.99997
Product of squares of normal-mode angular frequencies, $\omega_+^2 \omega_-^2$, in s^{-4}
Modeled inverse inertia, in $(kg\ m^2)^{-1}$
0
5
10
15
20
25
30
35
40
0
2000
4000
6000
8000

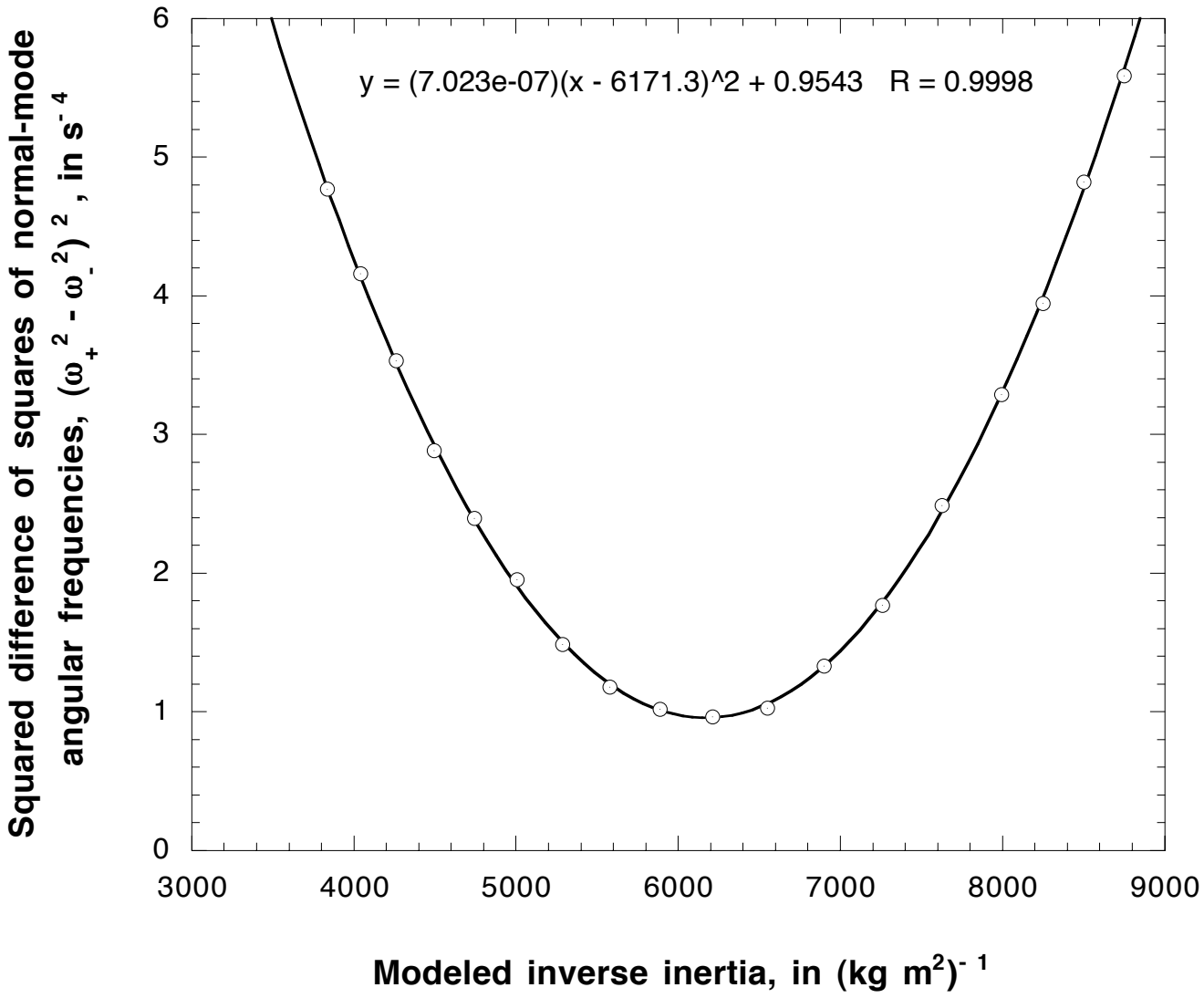
y = (7.023e-07)(x - 6171.3)^2 + 0.9543 R = 0.9998
Squared difference of squares of normal-mode angular frequencies, $(\omega_+^2 - \omega_-^2)^2$, in s^{-4}
Modeled inverse inertia, in $(kg\ m^2)^{-1}$
0
1
2
3
4
5
6
3000
4000
5000
6000
7000
8000
9000

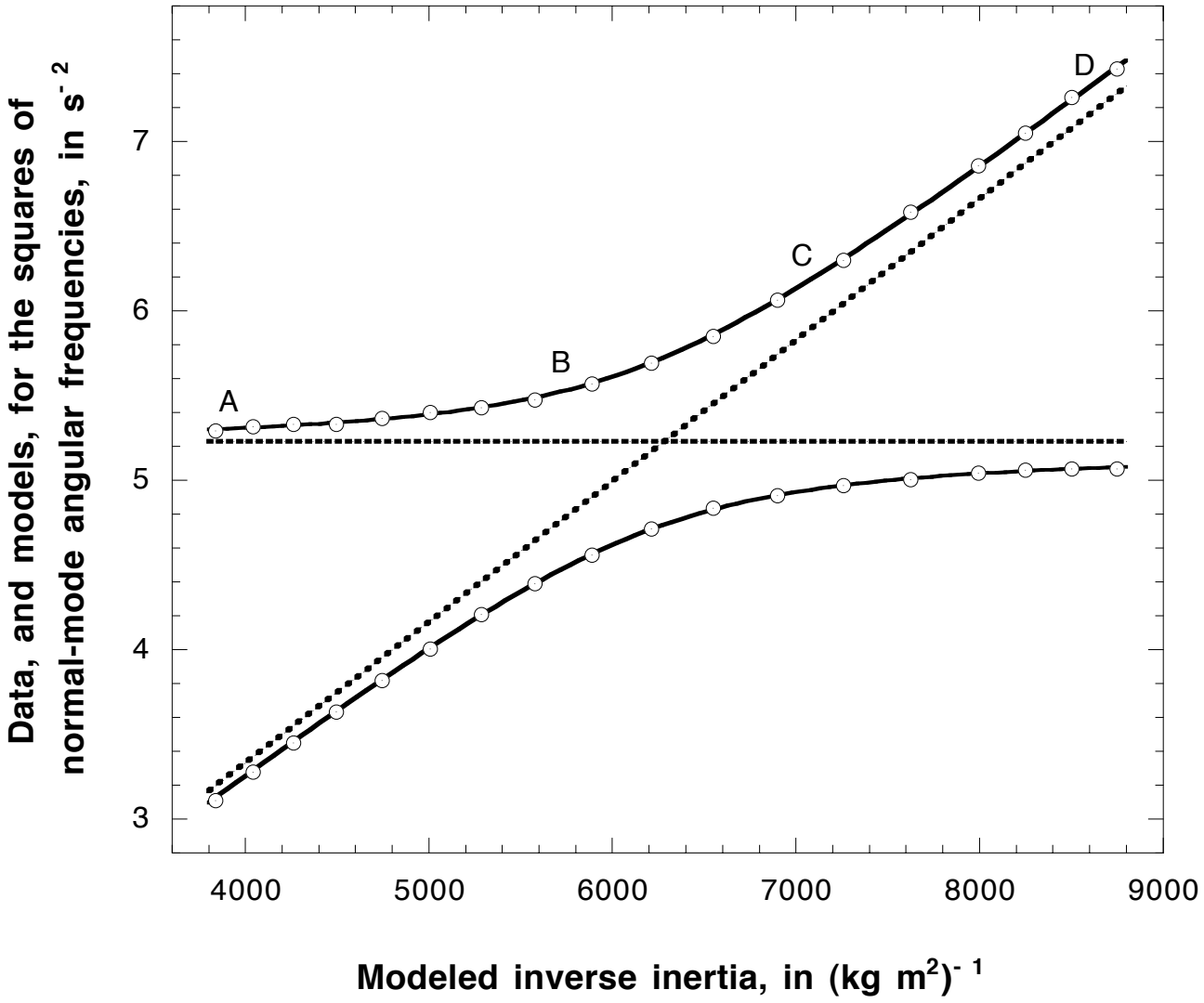
Data, and models, for the squares of normal-mode angular frequencies, in s^{-2}
Modeled inverse inertia, in (kg m^2)$^{-1}$
A
B
C
D
3
4
5
6
7
4000
5000
6000
7000
8000
9000

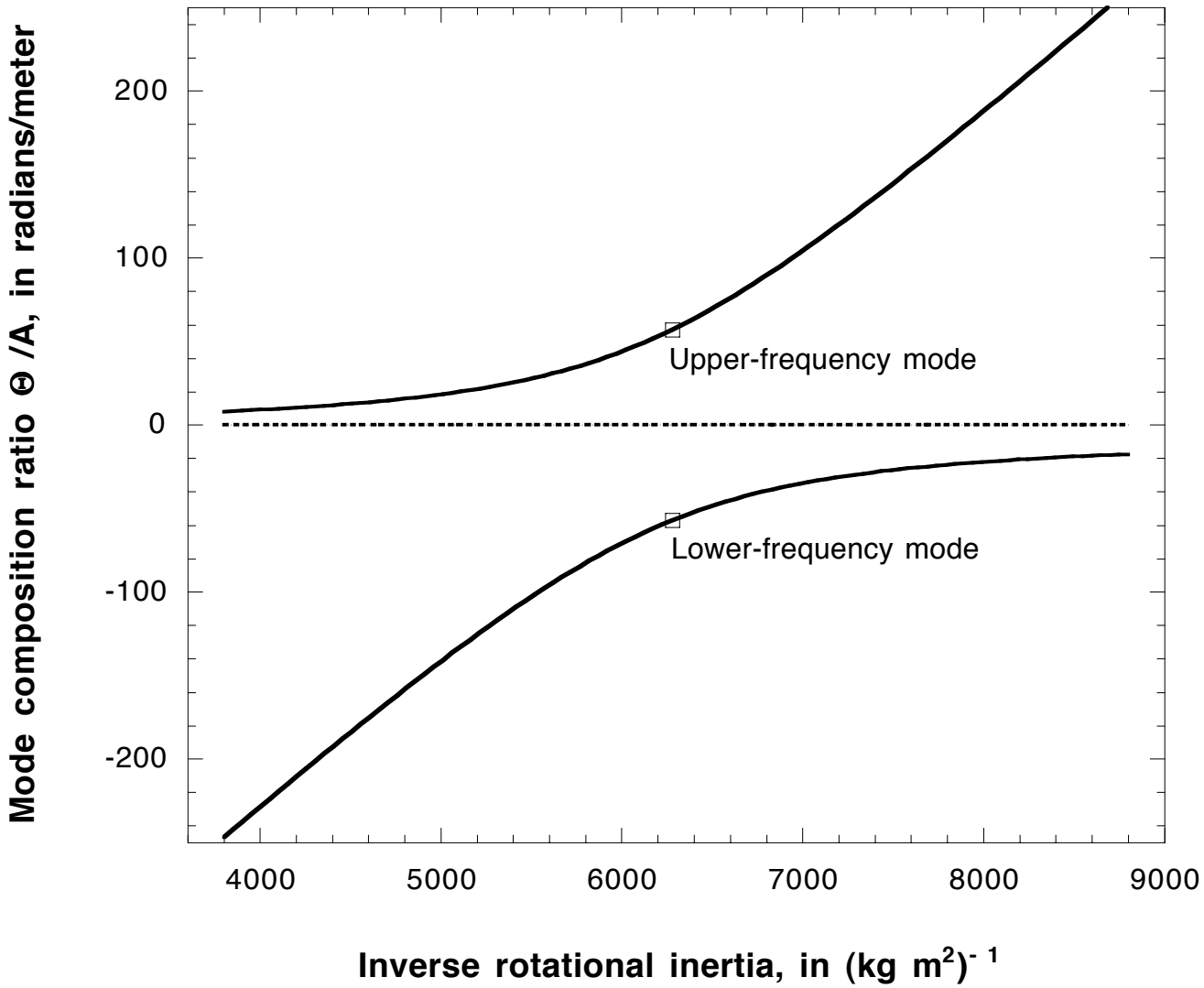
Mode composition ratio Θ /A, in radians/meter
200
100
0
-100
-200
Upper-frequency mode
Lower-frequency mode
4000
5000
6000
7000
8000
9000
Inverse rotational inertia, in (kg m²)⁻ ¹

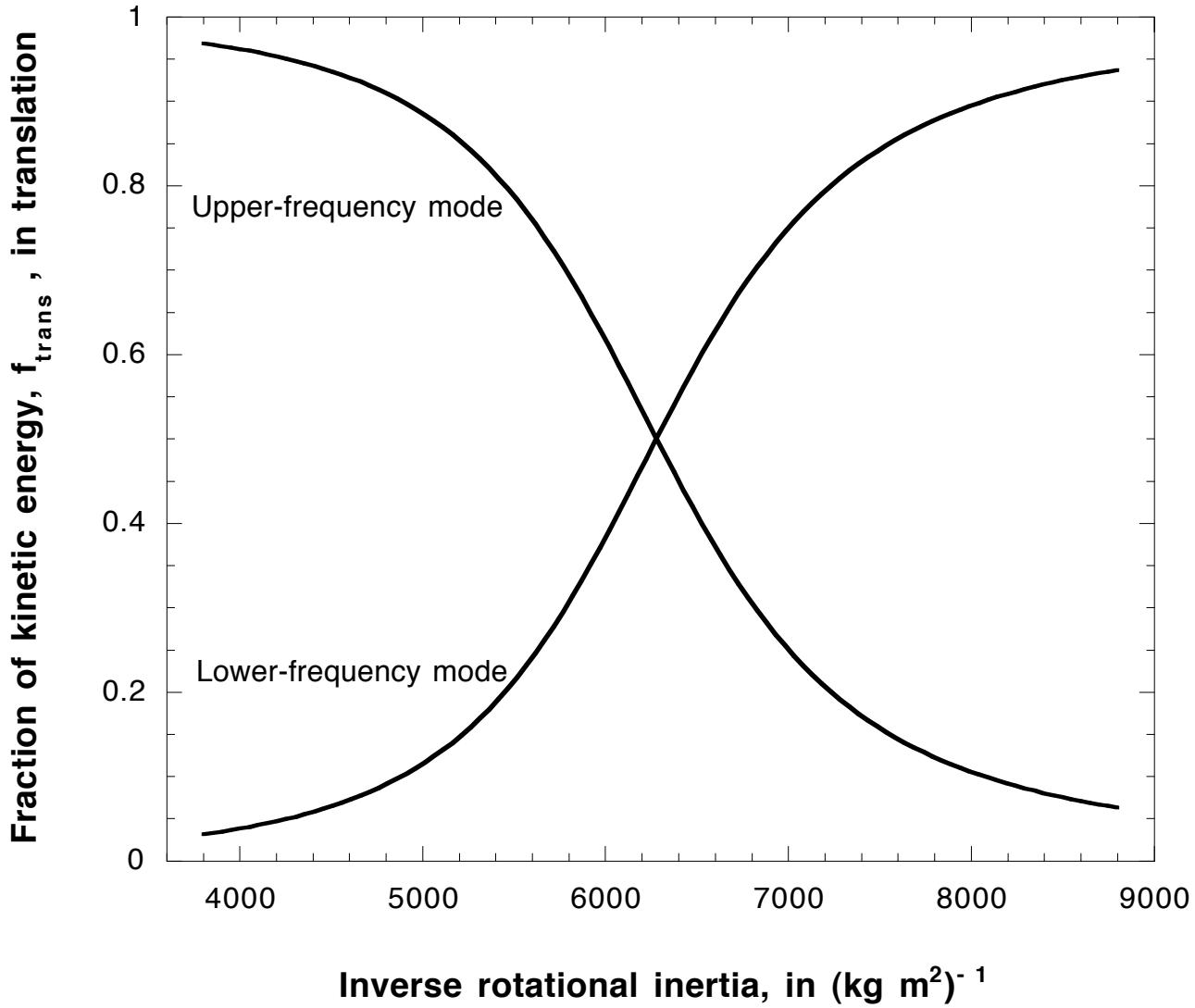
Fraction of kinetic energy, f_{trans}, in translation
1
0.8
0.6
0.4
0.2
0
Upper-frequency mode
Lower-frequency mode
4000
5000
6000
7000
8000
9000
Inverse rotational inertia, in $(kg\ m^2)^{-1}$